PORT SAID ENGINEERING RESEARCH JOURNAL
Faculty of Engineering - Port Said University
Volume 26 No. 1 pp: 68:83

Effect of Geometrical Properties of Aluminum Extrusion on Post-Buckling Behavior of Stiffened Panels in Marine Applications

*M.A. El-Malaki[1], *, S. Saad-Eldeen[2] and H.S. El-Kilani[3]*

[1] *Shipbuilding Engineer, Port Said Shipyard, Suez Canal Authority, Port Said, Egypt, email: Mohamed.elmalaki@suezcanal.gov.eg*

[2] *Associate Professor, Naval Architecture and Marine Engineering Department, Faculty of Engineering, Port Said University, Port Said, Egypt, email: saad.bahey@eng.psu.edu.com*

[3] *Professor, Naval Architecture and Marine Engineering Department, Faculty of Engineering, Port Said University, Port Said, Egypt, email: hebaelkilani@eng.psu.edu.com*

* *M.A. El-Malaki,* Mohamed.elmalaki@suezcanal.gov.eg, *DOI: 10.21608/pserj.2021.92580.1137.*

Received 25-8-2021
Revised 8-9-2021
Accepted 14-9-2021

ABSTRACT

The aim of the present paper is to define guidelines for the appropriate selection of the optimal geometrical characteristics for different aluminum extruded profiles based on the ultimate load carrying capacity as well as the post-collapse deformed shape of stiffened panels. A series of finite element analysis has been conducted for stiffened aluminum panels subjected to uniaxial compressive load; the master model has been validated based on full-scale experimental test results. The effect of open and closed section dimensions on the ultimate compressive capacity has been investigated. The analyses are performed for several cross-sections classified in groups, all with the same plate and column slenderness. The numerical results obtained are compared with the design capacity according to European standard for aluminum structures, Eurocode 9. Based on the comparative analysis, several concluding remarks ad recommendations which are benefit both design and repair strategies are summarized, and a criterion has been proposed for selecting the best cross-section considering both load carrying capacity and cross-section weight.

Keywords: Aluminum; Extrusion; Post-buckling; Stiffened Panels; Geometrical Properties.

1. INTRODUCTION

Stiffened aluminum plates consisting of welded extrusions are commonly used in high-speed ferries and ship superstructures, as well as living quarters on offshore installations. Other applications are plate girders, containers, and bridge decks. This development has primarily been driven by the demand for reduced weight, increased payload, higher speed, and reduced fuel consumption.

Little [1] analyzed the collapse behavior of simply supported rectangular aluminum plates, subjected to uniaxial compressive load. The effect of plate slenderness, initial imperfections and stress-strain curve knee factor on the ultimate capacity are investigated. It was concluded that the effect of initial imperfection is considerable for plate slenderness less than 1.5. Also, the knee factor has less effect on the ultimate strength.

Butler et al. [2] performed compressive experimental tests on five aluminum stiffened panels. It was observed that there is an interaction between the buckling modes, which directly affects the prediction of the final failure form.

Paik et al. [3] developed empirical expressions for predicting the ultimate compressive strength for aluminum panels as function of plate and column slenderness.

Khedmati et al. [4] carried out sensitivity analysis on the post-buckling behavior of aluminum stiffened plates, subjected to combined load. It was concluded that as the HAZ width in the plate increases, the ultimate strength decreases bilinearly regardless the lateral load value.

Rønning et al. [5] investigated experimentally the ultimate compressive strength of 21 stiffened aluminum panels with both closed and open stiffener sections. Two failure modes, local interframe and global flexural are observed. The panels with open stiffener sections showed satisfactory post-buckling strength on contrary to the panels with closed sections.

Zareei et al. [6] performed a series of elastoplastic large-deflection analyses of stiffened aluminum plates and applied artificial neural network to predict the ultimate compressive strength.

Tawosy et al. [7] investigated the effect of initial imperfection, aspect ratio, and column slenderness on the ultimate strength of the aluminum stiffened panel under combined load. It has been found that for imperfected panels the increase of aspect ratio affects the ability of the panel to withstand the applied load.

Mohammadi et al. [8] estimated the elastic local buckling of stiffened aluminum plates, considering both initial deflection and residual stresses. A modification of the energy-method-based Fujikubo–Yao's algorithm is also presented.

Tryland et al. [9] performed a series of mechanical properties tests; tensile and compressive on extrusion aluminum with varied sections and extrusion directions. It was concluded that orientation of the specimens relative to extrusion axis 90o shows the highest strength, while the one with 45o provides the lowest strength. Also, the strain hardening of the thick square hollow section is significantly lower than the thinner one as well as for the double tee section.

The European Committee for Standardization (CEN) has developed a series of model building codes, designed to eventually replace national building codes in the European Union. Eurocode 9 [10] dealt with the design of aluminum structures, and contains formulations for the ultimate strength of plates.

Section classification, which addresses the susceptibility of a cross section to local buckling and defines its appropriate design resistance [11], is established by Eurocode 9 according to the slenderness parameter as follow:

a) Class 1 no buckling occurs.
b) Class 2 buckling occurs after the compressed element has been plastically deformed to a strain, which is more than about twice the strain corresponding to the f0.2.
c) Class 3 buckling occurs once the 0.2 proof strength has been reached.
d) Class 4 buckling occurs before the average stress in the compressed part of the section has reached the 0.2 proof strength.

Eurocode 9 [12] has been found conservative in general as a result of ignoring the benefit of element interaction as it treats cross-sections on an element by element basis, and utilizes an elastic-perfectly plastic material model, excluding the beneficial influence of strain hardening.

Liu et al. [13] reviewed the recent research on the ultimate compressive strength of aluminum plates and stiffened panels, considering the effect of boundary condition, initial imperfection, welding-induced residual stress, and heat-affected zone. Also, the effect of manufacturing technology on the ultimate strength has been investigated numerically, concluding that the integrated extruded stiffened panel enhanced the strength than the one of the traditional welded panels.

The aim of the present paper is to study the influence of panel geometrical properties; attached plate thickness, stiffener web thickness, stiffener flange thickness, stiffener flange width and stiffener web height on buckling and post-collapse behavior of the panel under uniaxial compressive load is investigated. A comparison between the FEM results of a validated stiffened panel of closed section HAT, fabricated for high-speed catamarans will be carried out using different closed and open cross-sections of the stiffener. It is intended to propose a criterion to select the optimal extruded section for approximately 36 configurations based on maximum load carrying capacity with maximum section weight reduction.

2. REFERENCE MODELS AND VALIDATION

The reference models for the current study are based on a series of tests carried out by Aalberg [14] for aluminum stiffened panel considering two types of extruded profiles; open section of L-shape and closed section of HAT-shape, with different geometrical configurations and material properties, as shown in Fig. 1 and given in Table 1. Both panels represent a floor of catamaran passenger deck.

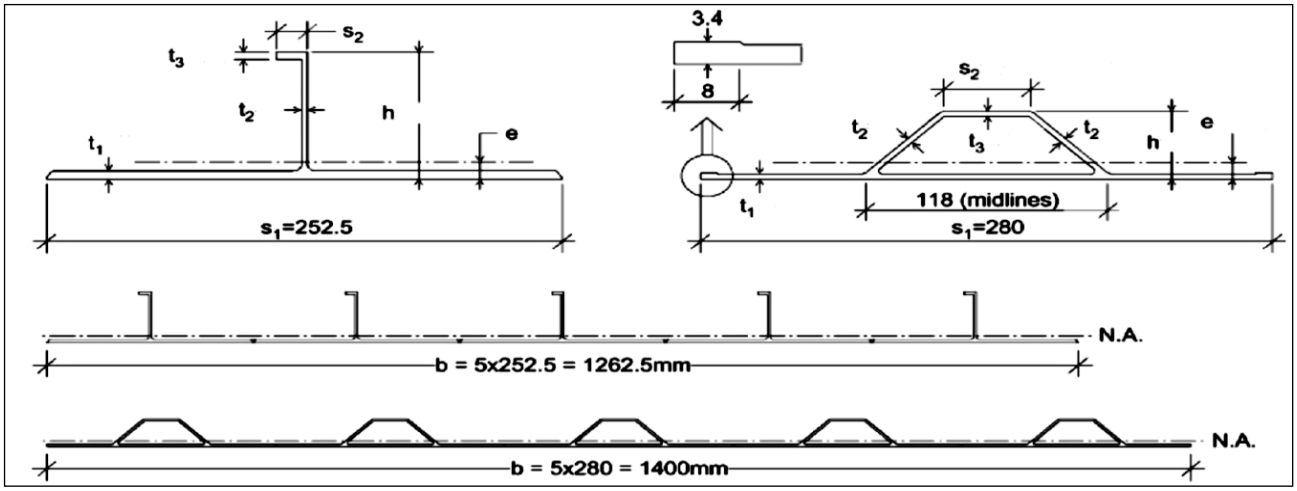

Fig. 1 Cross-sectional geometry of extruded profiles and cross-sections of gross panels, [14]

Table 1 Geometrical configurations and material properties of reference models, [14]

Stiffener section	a, b [mm]	σ_y [MPa]		Cross-section [mm]						Imperfections [mm]				
		Plate	Stiffener	t_1	t_2	t_3	s_1	s_2	h	ω_1	ω_2	ω_3	ω_4	ω_5
Closed	2000, 1400	261	275	3.10	3.08	3.04	280	42	41.1	1.9	1.4	2.9	2.4	0.2
Open	2000, 1262.5	254	270	4.87	2.97	4.37	252.5	14.9	76.5	2.5	3.0	3.5	3.0	2.0

The test has been conducted using an actuator with a capacity of 2500 kN, where the panels are mounted vertically, and the axial compressive load is applied along the edges through a stiff loading beam and the lower edges works as reaction supports. The test has been carried out with a displacement control of 1.0 mm/min. The imposed boundary conditions along the four edges according to the experimental set up for the selected reference models are given in Fig. 2.

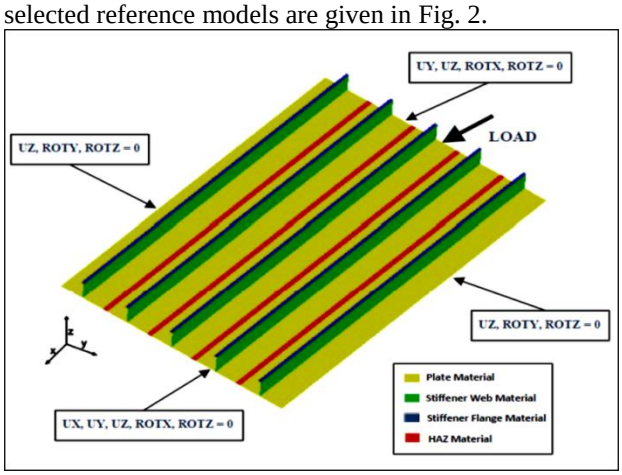

Fig. 2 Boundary conditions according to the experimental set up

According to the test conditions and real fabrication processes, both plates and stiffeners are made of different material grades, showing mean yield stress based on tensile test results of 286 and 272 MPa for closed section (HAT) and 309 MPa, 302 MPa for open section (L). To perform the intended FEM, the stress-strain curve of both plate and stiffeners has been implemented by using the original stress-strain curve data with bilinear behavior of the material, considering elastic modulus of 70 GPa.

The entire FE models have been generated using SHELL181, which is suited for buckling and nonlinear analysis with six degrees of freedom. The actual measured initial imperfections for the two reference models are tabulated in Table 1. Within the entire FEM a simplified imperfection distribution is used based on Fourier components [15]. The simplified value of the initial imperfection amplitude is calculated according to the following expression defined by [3]:

For plating, the initial imperfection distribution may follow the given expression:

$$W_{opl} = A_0 \, Sin \, \frac{m \pi x}{a} \, Sin \, \frac{\pi y}{b} \tag{1}$$

Where A_0 is the imperfection amplitude, which may be calculated as for average level, $0.096\beta^2 t$, a is the plate length between transverse frames, b is the breadth between longitudinal stiffeners and m is the number of half-waves in the longitudinal direction. For stiffeners, the column type initial distortion distribution of the stiffener may follow the following expression:

$$W_{oc} = B_0 \, Sin \, \frac{\pi x}{a} \, Sin \, \frac{\pi y}{B} \tag{2}$$

Where B_0 is maximum the imperfection amplitude, which may be calculated as for average level, 0.0018a.

Considering the sideway initial distortion of the stiffener, the distribution may be as follow:

$$W_{os} = C_0 \, \frac{Z}{h_w} \, Sin \, \frac{\pi x}{a} \tag{3}$$

Where C_0 is the maximum imperfection amplitude, which may be calculated as for average level, 0.001a, h_w is the height of stiffener.

Fig. 3 and Fig. 4 shows the plot of actual and simplified initial imperfection for both reference models, closed section B and open section J.

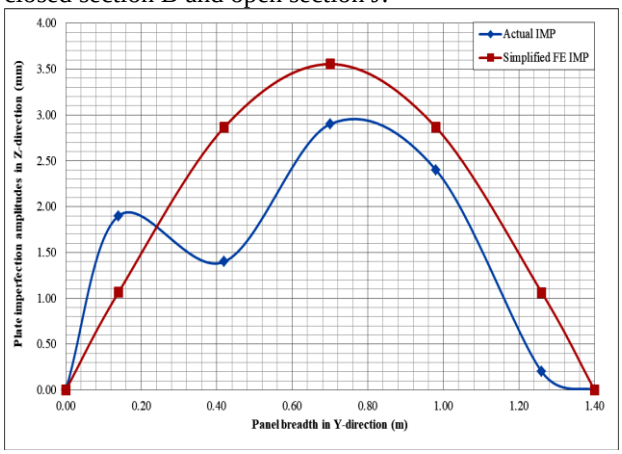

Fig. 3 Actual vs. simplified plate initial imperfection for closed model

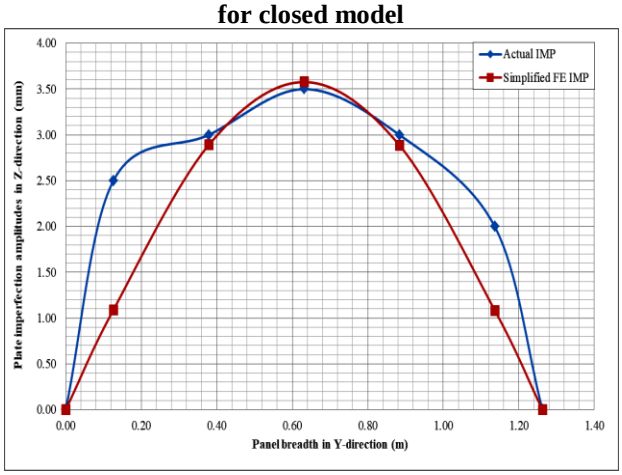

Fig. 4 Actual vs. simplified plate initial imperfection for open model

2.1. Calibration of Finite Element Model

The finite element analysis is performed in two steps, the first one with initial imperfection with different element sizes, to find out the best mesh design. Several element sizes as (5mm, 10mm, 15mm, 20mm, 25mm, 30mm, 35mm, and 40mm) are considered for the analysis for both reference models. It was found that for the present FE analysis, the most appropriate element size is 30 x 30 mm for closed and open reference models.

The load shortening curves for both experimental model and the FE one for closed and open section are shown in Fig. 5 and Fig. 6, respectively.

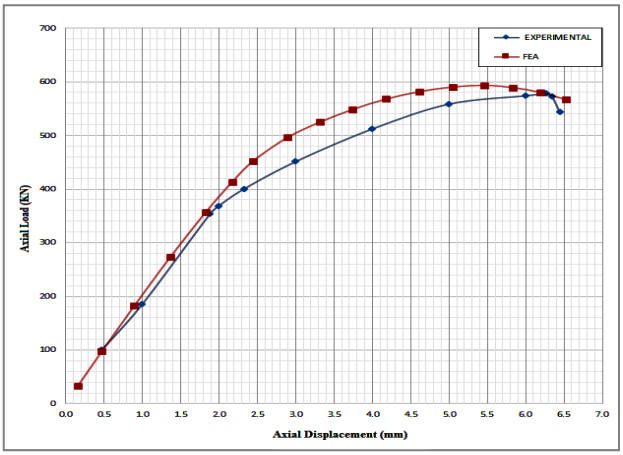

Fig. 5 Experimental VS. FEA results for closed section model

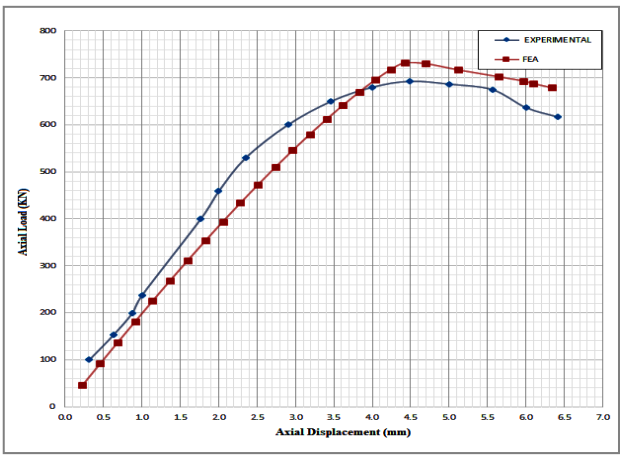

Fig. 6 Experimental VS. FEA results for open section model

3. FINITE ELEMENT ANALYSIS

The relevant cross-sections of the attached stiffener considered for the present analysis are shown in Fig. 7; flat bar (I), angle (L), and tee sections (TEE). The finite element analysis have been carried out using the commercial code ANSYS, [16].

The ultimate strength of stiffened panels subjected to uni-axial compressive load is governed by the following parameters:

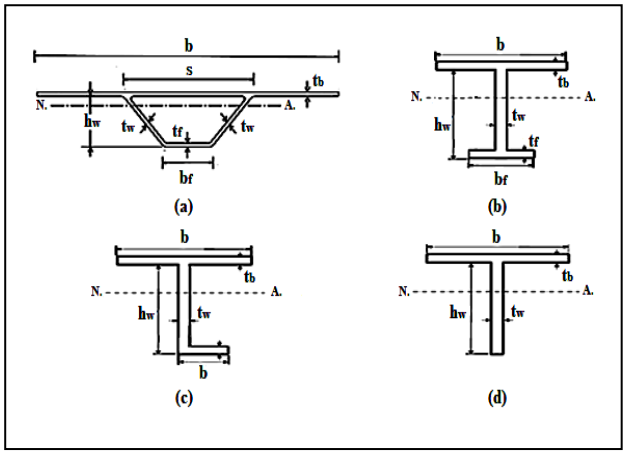

Fig. 7 Cross-sections of extruded stiffeners. (a) HAT, (b) TEE, (c) ANGLE and (d) FLAT bar

$$\text{Plate slenderness: } \beta = \frac{b}{t_p}\sqrt{\frac{\sigma_y}{E}} \quad (4)$$

$$\text{Column slenderness: } \lambda = \frac{a}{\pi r}\sqrt{\frac{\sigma_y}{E}} \quad (5)$$

where: a is the plate length between transverse frames, b is the plate breadth between longitudinal stiffeners, tp is the plating thickness, I is the moment of inertia of the plate-stiffener combination, A is the plate-stiffener combination cross-sectional area, r is the radius of gyration, σ_y is the material yield stress and E is the modulus of elasticity.

In the present work, a series of FEA is performed to investigate the influence of different geometrical parameters of four stiffener cross-sections shown in Fig. 7, on the collapse load of aluminum stiffened panel. Two governing parameters; plate slenderness (β) and column slenderness (λ) are kept constant, whereas different values for the different relations between plating thickness (t_p), web thickness (t_w) and flange thickness (t_f), are attributed to each case. The resulting 36 panels are categorized as follow, 11 panels for each stiffener type except the FLAT bar, where only 3 panels are considered due to the absence of having flange, as described in Table 2.

The following constraints have been respected in the selection of extruded stiffeners dimensions:

a) The design variables lower bounds for closed and open sections which selected to ensure that the cross-sections would be extrudable in 6082-T6 material [17].
b) The ratio of maximum thickness in the section to minimum thickness shall be kept at less than 2:1 to ensure that the section is practical to extrude [17].
c) Achievable minimum cross sections weight and maximum section modulus.
d) Avoid slender member as possible in the selection of web height and flange width according to EC9 buckling classification [10], i.e. the member buckling class < 4.

The length, breadth, thickness and frame spacing of the panels are kept constant similar to the reference panel [14].

The geometrical characteristics of the panels considered, with constant plate and column slenderness of 5.70 and 1.80, respectively, are given in Table 3.

Table 2 Description of different groups and cases

Groups		Stiffener cross-sections			
		HAT (H)	HAT (H)	HAT (H)	HAT (H)
A	A1	$t_p = t_w = t_f$	Same as HAT		$t_p = t_w$
B	B1	$t_p = t_w > t_f$			
	B2	$t_p = t_w < t_f$			
C	C1	$t_p = t_f > t_w$			
	C2	$t_p = t_f < t_w$			
D	D1	$t_p > t_w = t_f$			$t_p > t_w$
	D2	$t_p < t_w = t_f$			$t_p < t_w$
E	E1	$t_p > t_w > t_f$			
	E2	$t_p > t_f > t_w$			
	E3	$t_p < t_w < t_f$			
	E4	$t_p < t_f < t_w$			
Total number for cases		11	11	11	3

Table 3 Geometrical characteristics of the panels (L = 2000 & B = 1400)

Panel ID	Extrusion Dimensions, mm b = 280 & t_p = 3					Z, cm^3	Section Weight (kg/m)	EC9 Buckling Class	
	h_w	t_w	b_f	t_f	s			Web	Flange
Ref.	38.00	17.40	3.48	3.00	118.00	17.40	3.48	2	2
H-A1	37.00	19.35	3.39	3.00	70.00	19.35	3.39	2	3
T-A1	63.00	10.16	3.06	3.00	--	10.16	3.06	3	3
L-A1	67.00	9.35	3.02	3.00	--	9.35	3.02	3	4
I-A1	84.00	6.83	2.95	--	--	6.83	2.95	--	4
H-B1	39.00	16.64	3.29	2.50	70.00	16.64	3.29	2	3

T-B1	66.00	9.53	3.03	2.70	--	9.53	3.03	3	3
L-B1	67.00	9.39	3.02	2.80	--	9.39	3.02	3	4
H-B2	36.00	20.78	3.46	3.50	70.00	20.78	3.46	2	3
T-B2	59.00	11.35	3.13	3.50	--	11.35	3.13	3	3
L-B2	68.00	9.00	3.01	3.50	--	9.00	3.01	3	3
H-C1	37.50	18.75	3.29	3.00	69.00	18.75	3.29	2	3
T-C1	63.00	9.96	3.03	3.00	--	9.96	3.03	3	3
L-C1	63.00	10.14	3.04	3.00	--	10.14	3.04	3	4
H-C2	36.50	19.89	3.48	3.00	71.00	19.89	3.48	1	3
T-C2	63.00	10.66	3.14	3.00	--	10.66	3.14	3	3
L-C2	70.00	9.01	3.07	3.00	--	9.01	3.07	3	3
H-D1	40.00	16.19	3.20	2.50	69.00	16.19	3.20	2	3
T-D1	64.00	9.90	3.04	2.90	--	9.90	3.04	3	3
L-D1	60.00	10.97	3.07	2.70	--	10.97	3.07	3	4
I-D1	88.00	6.29	2.86	--	--	6.29	2.86	--	4
H-D2	36.00	21.69	3.55	3.50	71.00	21.69	3.55	1	3
T-D2	59.00	11.76	3.21	3.50	--	11.76	3.21	3	3
L-D2	67.00	9.59	3.09	3.50	--	9.59	3.09	3	3
I-D2	74.00	9.42	3.37	--	--	9.42	3.37	--	4
H-E1	42.50	13.96	3.13	2.00	69.00	13.96	3.13	3	3
T-E1	65.00	9.57	3.02	2.80	--	9.57	3.02	3	3
L-E1	63.00	10.09	3.03	2.60	--	10.09	3.03	3	4
H-E2	40.50	15.36	3.10	2.50	68.00	15.36	3.10	3	3
T-E2	63.00	10.10	3.04	2.90	--	10.10	3.04	3	4
L-E2	58.00	11.45	3.09	2.80	--	11.45	3.09	3	4
H-E3	35.00	22.88	3.62	4.00	71.00	22.88	3.62	1	3
T-E3	56.00	13.16	3.30	4.00	--	13.16	3.30	2	3
L-E3	64.00	10.23	3.13	4.00	--	10.23	3.13	3	3
H-E4	35.50	22.12	3.64	3.50	72.00	22.12	3.64	1	3
T-E4	59.00	12.36	3.29	3.50	--	12.36	3.29	2	3
L-E4	67.00	10.14	3.18	3.50	--	10.14	3.18	3	3

The relevant collapse modes for stiffened plates subjected to uniaxial compression may be summarized as plate induced overall buckling (PI), stiffener induced overall buckling (SI), plate buckling (PB) and stiffener tripping (ST).

Due to the criticality of the stiffener stiffness, which affects directly the buckling behavior, several studies investigate the effect of axial, flexural and torsional stiffness of the stiffener on the strength of aluminum stiffened panels as [3], [18] and [19]. The stiffness components may be calculated as:

$$\text{Axial stiffness: } A_S = \frac{EA}{L} \quad (6)$$

$$\text{Flexural stiffness: } F_S = \frac{EI}{L} \quad (7)$$

$$\text{Torsional stiffness: } T_S = \frac{GJ}{L} \quad (8)$$

Where G is the shear modulus, J is the polar moment of inertia of the plate-stiffener combination and L is the stiffener unsupported length.

3.1. FE Results for Group A

The relationship between axial load-displacement for the four considered stiffener cross-sections with equal thicknesses of plating (tp), web (tw) and flange (tf) are presented in Fig. 8 (left), with corresponding deformed shapes at ultimate load step shown in Fig. 9. The reference panel is denoted as Ref., which represents the FEM results of closed section stiffeners panel (HAT stiffeners).

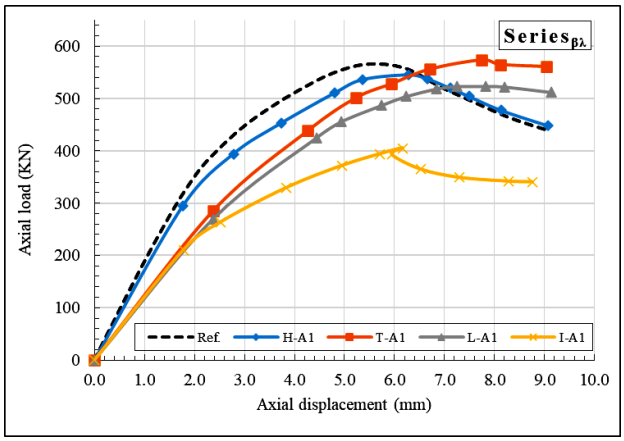

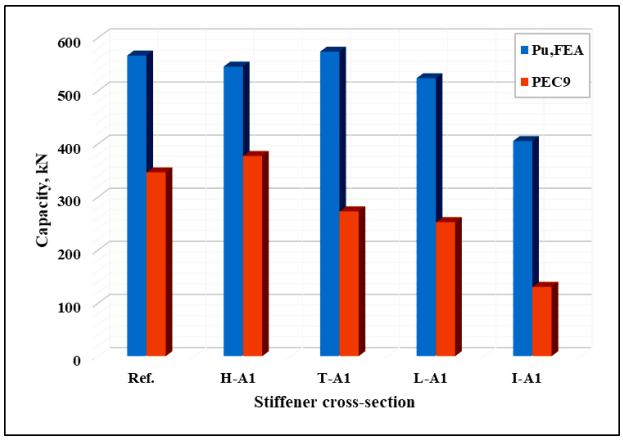

Fig. 8 Load shortening curve (left) and ultimate compressive capacity FEA vs design resistance EC9 (right), Group A1

As may be seen from Fig. 8 and Table 4, three cross-sections: H-A1, T-A1, and L-A1 showed capacities differences with respect to the Ref. model as -3.68%, +1.27% and -7.55%, respectively. While the fourth section I-A1, registered the lowest ultimate capacity with - 28.46%. This agrees with the resultant deformed shapes presented in Fig. 9, where the developed failure mode for I-A1 cross-section is stiffener tripping ST caused by the failure of the stiffener to withstand the transmitted load from the plate. For the other sections, the developed failure modes are PI, PB and PB, respectively, see Fig. 9, where H-A1 of PI agrees with the one observed during the experimental test of the Ref. model.

Therefore, it may be stated that for the first group of the analysis (A1); from ultimate capacity point of view, the flat bar cross-section is not an appropriate cross-section. This coincides with the lower axial and torsional stiffness represented by I-A1 which are less than the Ref. one by 15.35% and 30.29%, respectively, which facilitate the development of stiffener tripping failure mode.

The obtained finite element results are compared with the design resistance formulations given by Eq. (9) Eurocode 9 [10].

$$P_{EC9} = \chi A_{eff} f_0 / \gamma_{M1} \quad (9)$$

Where χ is the reduction factor for flexural buckling, A_{eff} is the effective area of the cross-section, f_0 is the characteristic value of 0.2 % proof strength and γ_{M1} is the reduction factor obtained from the appropriate column curve relevant to column buckling of the sub-unit as a simple strut out of the plane of the plating.

Table 5 shows the calculated design resistance using Eurocode 9 and resultant ultimate compressive capacity using nonlinear FEA. As may be seen from Fig. 8 (right) and Table 5, the design resistance calculated by Eurocode 9 for all considered stiffener cross-sections is less than the obtained FEA results. This indicates that the design rules provide a safety factor that varies between 3.10 and 1.45 for the current analyzed series cross-sections, where the higher value corresponds to I-A1 and the lower value respects o H-A1, see Table 5.

The bias of Eurocode 9 is defined as the ratio between the design resistance and the ultimate compressive capacity, [20], where a bias value of 1.0 indicates a perfect prediction, < 1.0 conservative prediction, and > 1.0 non-conservative prediction.:

$$\text{Bias} = \frac{\text{Desgin resistance (PEC9)}}{\text{Ultiamte compressive capacity (Pu)}} \quad (10)$$

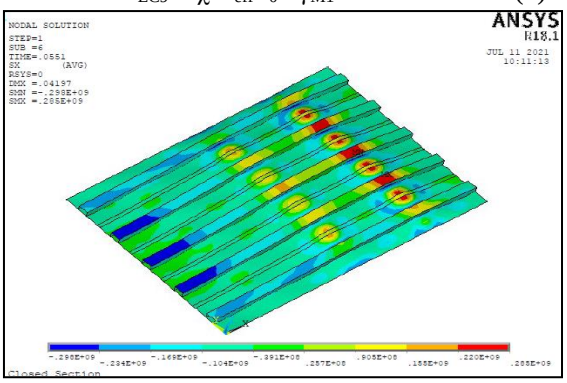

H-A (PI failure mode)

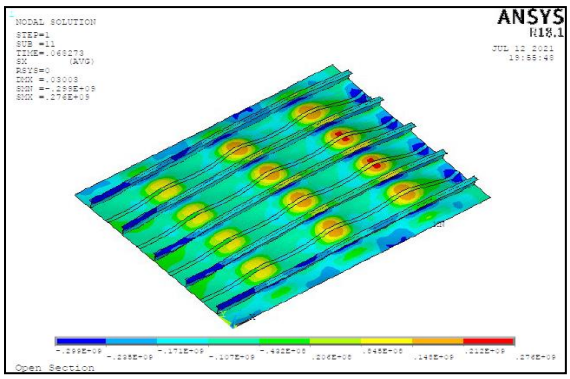

T-A (PB failure mode)

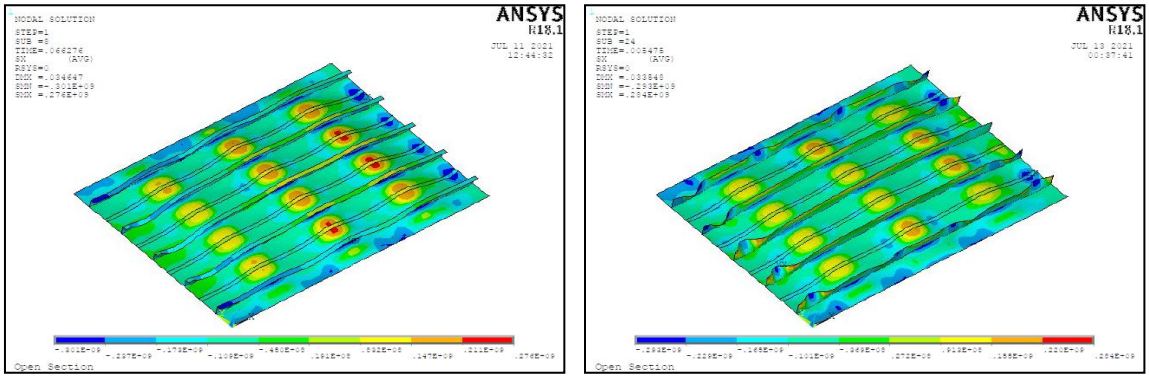

L-A (PB failure mode) I-A (ST failure mode)

Fig. 9 Deformed shapes at ultimate load, Group A

Table 4 Finite element analysis results, Group A1

Panel ID	Stiffness, kN.mm			P_u, kN	δa, mm	Diff. (P_u), %	Failure mode
	Axial, A_s	Flexural, F_s	Torsional, T_s				
Ref.	4.52E+03	1.80E+04	1.16E+05	566.31	5.46	--	PI
H-A1	4.39E+03	1.93E+04	9.57E+04	545.49	6.28	-3.68	PI
T-A1	3.97E+03	1.89E+04	8.16E+04	573.50	7.74	1.27	PB
L-A1	3.92E+03	1.89E+04	7.94E+04	523.58	7.82	-7.55	PB
I-A1	3.82E+03	1.80E+04	8.11E+04	405.16	6.16	-28.46	ST

Table 5 Comparison between FE results and Eurocode 9 [20]

Panel ID	FEA (Ultimate load) P_u, kN	Eurocode 9 (Design resistance) P_{EC9}, kN	Bias (P_{EC9}/P_u)	Safety factor S_f
Ref.	566.31	346.22	0.61	1.64
H-A1	545.49	377.13	0.69	1.45
T-A1	573.50	272.81	0.48	2.10
L-A1	523.58	252.59	0.48	2.07
I-A1	405.16	130.62	0.32	3.10

As given in Table 5, all values are less than 1 and varies between 0.69 and 0.32, indicating that the capacity prediction using Eurocode 9 is conservative. Regarding the structural weight as a key parameter for obtaining an optimal design option leading to an increase payload and reduce fuel consumption [21], Table 3 shows the weight of the panel for each stiffener cross-section. The closest section to the reference from weight point of view is H-A1 and the farthest one is I-A1.

Based on the performed analysis for group A1; FE, Eurocode 9 and weight calculations, a criterion for selecting best design option has been developed as presented in Fig. 10, for which the best option achieves both higher capacity as well as less weight, also the section may be accepted with ultimate capacity less than the Ref. one by 2%, which may result from convergence problem. Therefore, for the first group of the analysis (A1) the best design option is section T-A1 which provides higher capacity of (1.27%), safety factor of (2.10) according to Eurocode9 and reduced weight by (12.07%) with respect to the Ref. one.

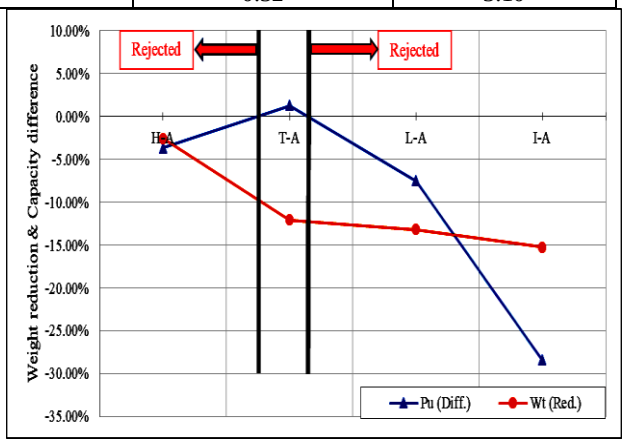

Fig. 10 Proposed criteria to select the optimum extruded section, GROUP A1

3.2. FE Results for Group B

For this group of the analysis, two geometrical variations are considered: Group B1 $t_p = t_w > t_f$ and Group B2 $t_p = t_w < t_f$.

3.2.1. Group B1

For this group of the analysis the geometrical variations are as follow for the three sections; the thickness of plating and web are equal, and both are bigger than the thickness of the flange ($t_p = t_w > t_f$).

The developed axial displacement corresponds to the applied axial load is shown in Fig. 11 (left). From ultimate capacity point of view, it is evident that both T-B1 and L-B1 are closer to the Ref. one with capacities

differences of -0.11% and -1.07%, respectively, see Fig. 11, but H-B1 results in lower capacity of -7.81%.

The developed failure modes for H-B1, T-B1 and L-B1 cross-sections are similar to those in group A1, with local buckling of the L-B1 panel flanges as shown in Fig. 12.

Regarding the slope of the load shortening curve, there is a big deviation between the Ref. and both T-B1 and L-B1 sections due to their lower axial stiffness as tabulated in Table 6, with developed higher axial displacement by 37.55% and 51.65% with respect to the Ref. one.

Fig. 11 (right) and Table 7 represent the resultant ultimate capacity of FEA and Eurocode 9 for Group B1 with the same notation of less calculated capacity by Eurocode 9, resulting in a safety factor between 1.49 and 2.22.

Fig. 13 represents a plot of the proposed criterion for selecting the best cross-section, which reveals that only section T-B1 may be considered as the best option with capacity difference with respect to the Ref. one by -0.11% and weight reduction of -12.93%.

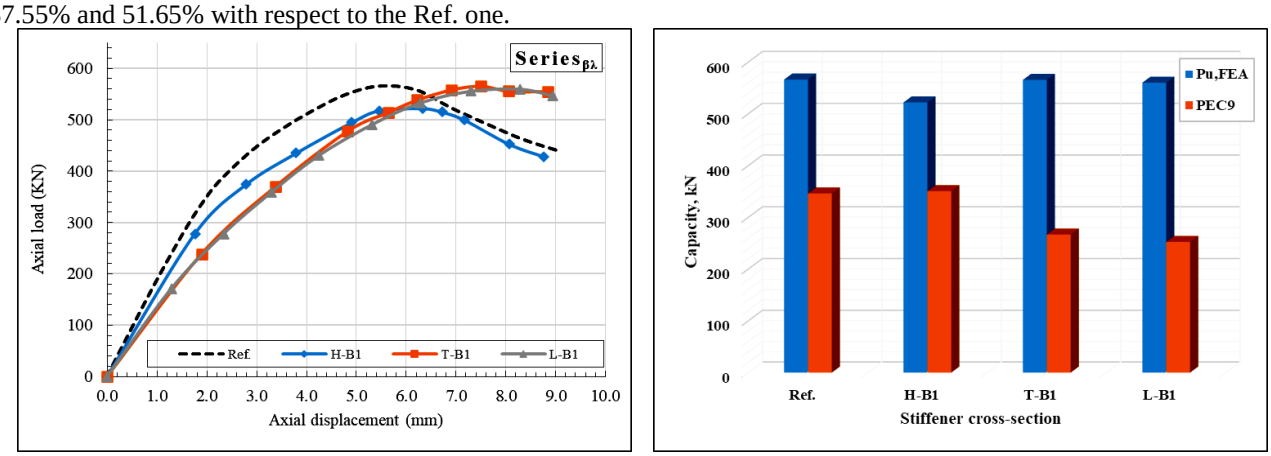

Fig. 11 Load shortening curve (left) and ultimate compressive capacity FEA vs design resistance EC9, Group B1

Table 6 Finite element analysis results, Series (βλB1)

Panel ID	Stiffness, kN.mm			P_u, kN	δa, mm	Diff. (P_u), %	Failure mode
	Axial, A_s	Flexural, F_s	Torsional, T_s				
Ref.	4.52E+03	1.80E+04	1.16E+05	566.31	5.46	--	PI
H-B1	4.27E+03	1.82E+04	9.41E+04	522.10	6.33	-7.81	PI
T-B1	3.93E+03	1.88E+04	8.15E+04	565.70	7.51	-0.11	PB
L-B1	3.92E+03	1.89E+04	7.94E+04	560.26	8.28	-1.07	PB

Table 7 Comparison between FE results and Eurocode 9

Panel ID	FEA (Ultimate load) P_u, kN	Eurocode 9 (Design resistance) P_{EC9}, kN	Bias (P_{EC9}/P_u)	Safety factor S_f
Ref.	566.31	346.22	0.61	1.64
H-B1	522.10	350.70	0.67	1.49
T-B1	565.70	266.80	0.47	2.12
L-B1	560.26	252.59	0.45	2.22

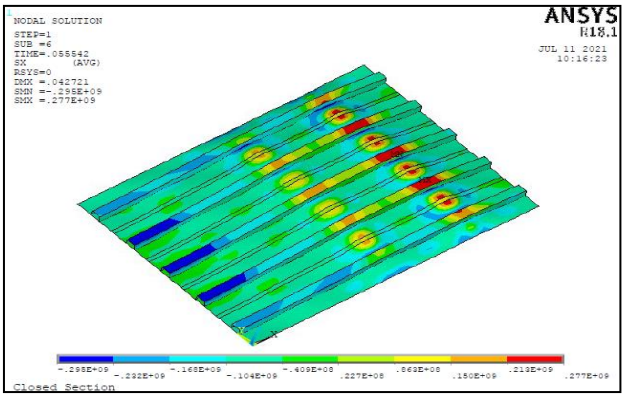

H-B1 (PI failure mode)

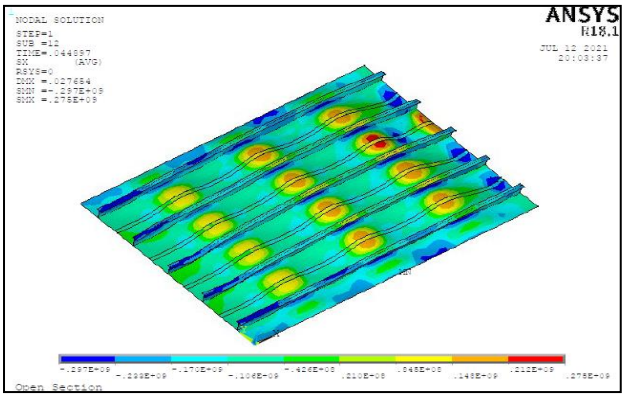

T-B1 (PB failure mode)

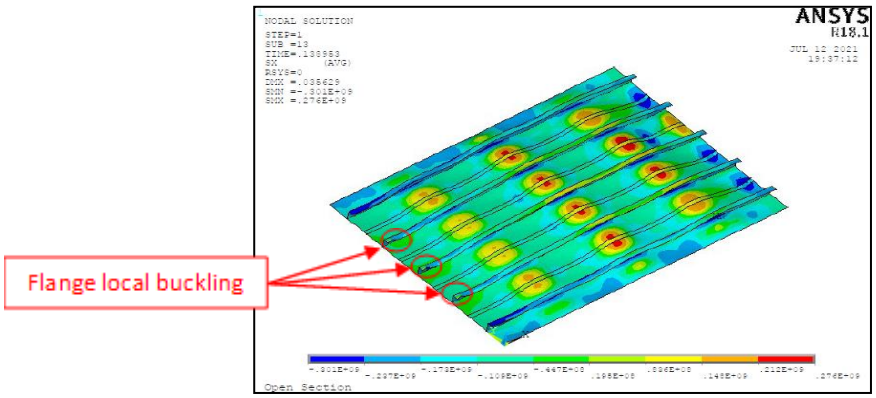

L-B1 (PB failure mode)

Fig. 12 Deformed shapes at ultimate load, Group B1

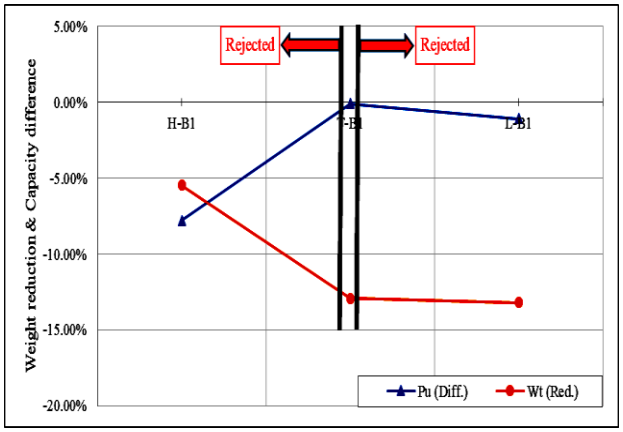

Fig. 13 Proposed criteria to select the optimum extruded section, GROUP B1

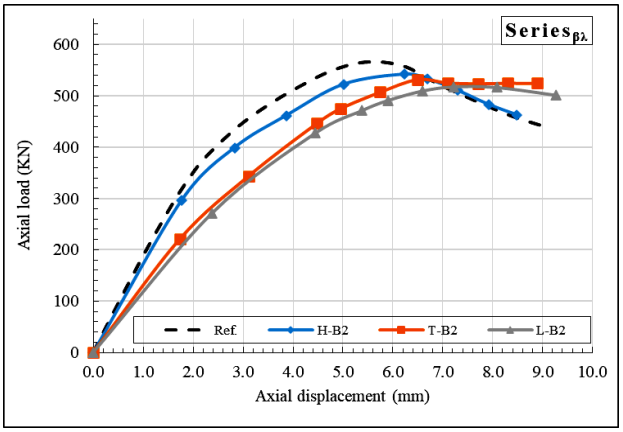

Fig. 14 Load shortening curve, Group B2

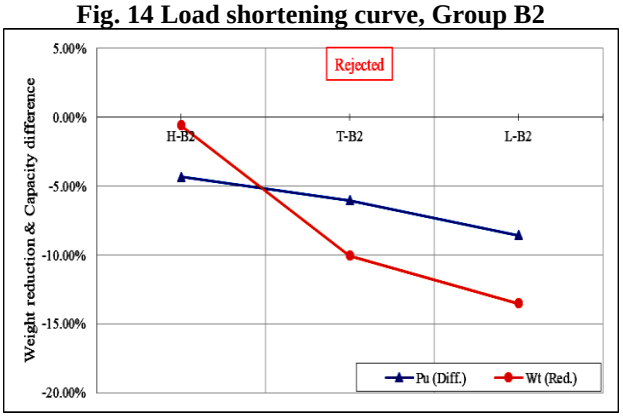

Fig. 15 Best section selection criteria, Group B2

3.2.2. Group B2

In this group, the geometrical variation is opposite to Group B1, where the flange thickness is less than both plating and web thicknesses ($t_p = t_w < t_f$).

The developed axial displacement corresponds to the applied axial load is shown in Fig. 14. As may be seen all sections H-B2, T-B2 and L-B2 show lower capacity than the Ref. one -4.32%, -6.04% and -8.55% respectively, see Fig. 14 and Table 8.

According to Fig. 15, it is clear that all cross-sections are rejected from ultimate capacity point of view.

Table 8 Finite element analysis results, Group B2

Panel ID	Stiffness, kN.mm			P_u, kN	Diff. (P_u), %	Eurocode 9 P_{EC9}, kN	Failure mode
	Axial, A_s	Flexural, F_s	Torsional, T_s				
Ref.	4.52E+03	1.80E+04	1.16E+05	566.31	--	346.22	PI
H-B2	4.48E+03	1.98E+04	9.60E+04	541.83	-4.32	385.62	PI
T-B2	4.06E+03	1.93E+04	8.19E+04	532.13	-6.04	289.79	PB
L-B2	3.90E+03	1.85E+04	7.85E+04	517.88	-8.55	260.52	PB

3.3. FE Results for Group C

In group C, the following geometrical variations are considered: Group C1 ($t_p = t_f > t_w$) and Group C2 ($t_p = t_f < t_w$). As may be seen from Fig. 16, for both groups C1 and C2, the response is almost the same for all sections with slight differences in the post collapse regime. Also, only section T-C1and T-C2 shows higher

capacity than the Ref. one by 0.32% and 2.28%, respectively and the difference between the two geometries is only the web thickness which gives higher resistance in case of T-C2. This agrees with the best selection creation which shows weight reduction of 12.93% and 9.77% for T-C1 and T-C2, respectively, see Fig. 17.

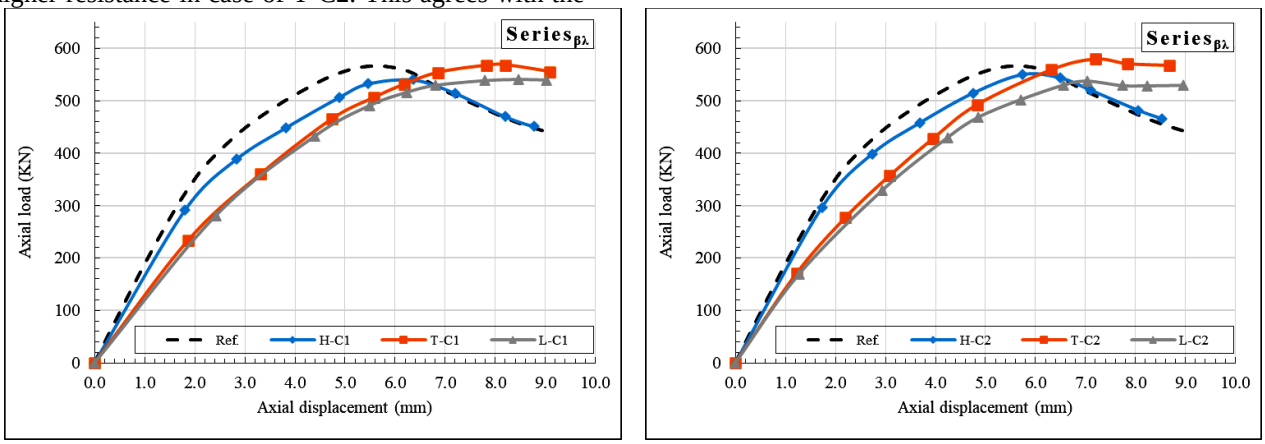

Fig. 16 Load shortening curve for Group C1 (left) and Group C2 (right)

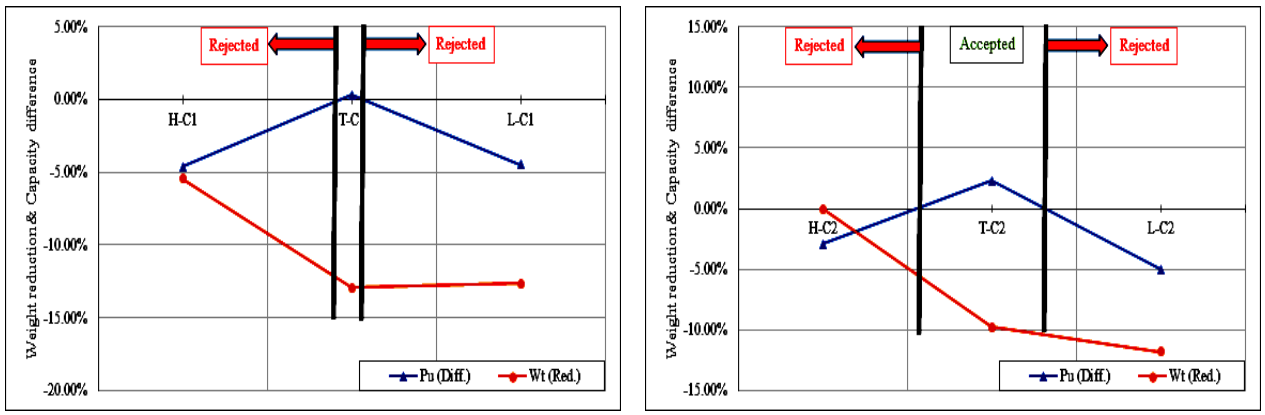

Fig. 17 Proposed criteria to select the optimum extruded section, Group C1 (left) and Group C2 (right)

Table 9 Finite element analysis results, Group C

Panel ID	Stiffness, kN.mm			P_u, kN	δa, mm	Diff. (P_u), %	Failure mode
	Axial, A_s	Flexural, F_s	Torsional, T_s				
Ref.	4.52E+03	1.80E+04	1.16E+05	566.31	5.46	--	PI
H-C1	4.27E+03	1.92E+04	9.37E+04	540.17	6.37	-4.62	PI
T-C1	3.93E+03	1.86E+04	8.15E+04	568.10	8.20	0.32	PB
L-C1	3.94E+03	1.89E+04	7.97E+04	540.95	8.46	-4.48	PB
H-C2	4.51E+03	1.94E+04	9.77E+04	549.85	5.75	-2.91	PI
T-C2	4.07E+03	1.96E+04	8.19E+04	579.24	7.20	2.28	PB
L-C2	3.98E+03	1.91E+04	7.87E+04	537.85	7.04	-5.03	PB

Table 10 Comparison between FE results and Eurocode 9, Group C

Panel ID	FEA (Ultimate load) P_u, kN	Eurocode 9 (Design resistance) P_{EC9}, kN	Bias (P_{EC9}/P_u)	Safety factor S_f
Ref.	566.31	346.22	0.61	1.64
H-C1	540.17	362.39	0.67	1.49
T-C1	568.10	265.05	0.47	2.14
L-C1	540.95	248.43	0.46	2.18
H-C2	549.85	382.98	0.70	1.44
T-C2	579.24	292.69	0.51	1.98
L-C2	537.85	275.76	0.51	1.95

3.4. FE Results for Group D

For group D, the thickness of the web and flange are equal, while the variation is related to the plating

thickness; Group D1 ($t_p > t_w = t_f$) and Group D2 ($t_p < t_w = t_f$) and the resultant axial load-displacement curve for both groups is presented in Fig. 18. It is evident that as the web and flange thickness is higher than the plating thickness, the global behaviour for all cross-sections improved nonlinearly especially with the ultimate carrying capacity. Also, this effect is clearly presented in cross-section I-D1 and I-D2, where the first one suffered from stiffeners tripping (ST mode) due to its lower flexural stiffness and the behaviour of the second one I-D2 enhances due to its higher flexural stiffness (PB mode) as may be seen from Fig. 19 and Table 11. It has to be stressed that only cross-sections T-D1 and T-D2 are the best options; with better choice of T-D2 due to its higher capacity and weight reduction with respect to the Ref. one by 1.05% and 7.76%, respectively.

This agrees with the resultant deformed shapes presented in Fig. 19, where the developed failure mode for I-D1 cross-section is stiffener tripping ST caused by the failure of the stiffener to withstand the transmitted load from the plate.

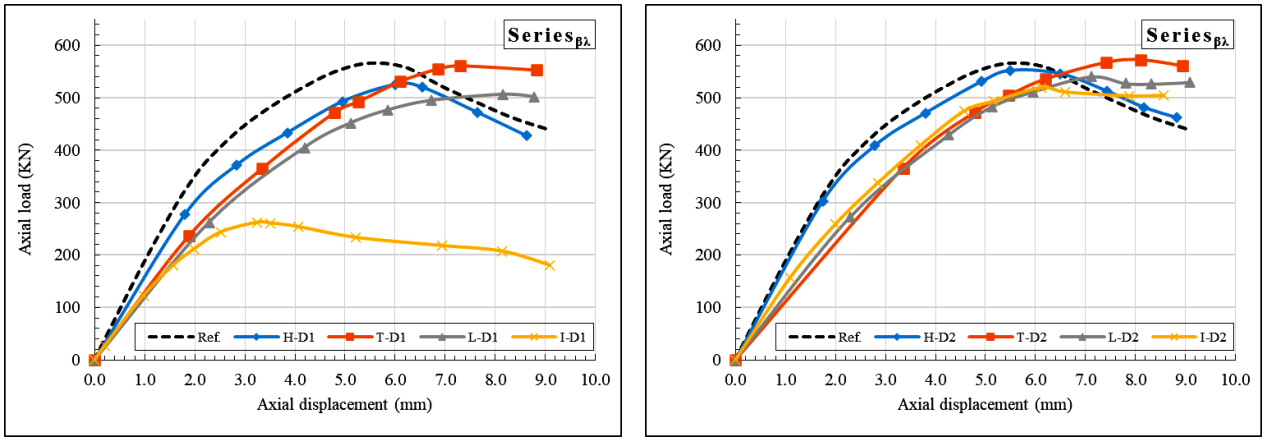

Fig. 18 Load shortening curve for Group D1 (left) and Group D2 (right)

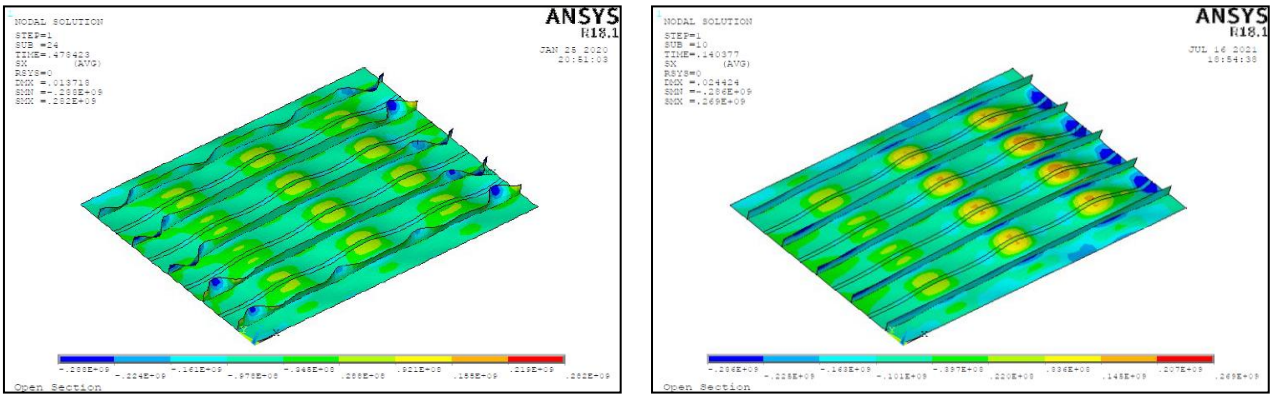

Fig. 19 Deformed shapes at ultimate load I-D1 (left) and I-D2 (right), Group D

Table 11 Finite element analysis results, Group D

Panel ID	Stiffness, kN.mm			P_u, kN	δa, mm	Diff. (P_u), %	Failure mode
	Axial, A_s	Flexural, F_s	Torsional, T_s				
Ref.	4.52E+03	1.80E+04	1.16E+05	566.31	5.46	--	PI
H-D1	4.15E+03	1.83E+04	9.24E+04	525.16	6.01	-7.27	PI
T-D1	3.94E+04	1.88E+04	8.15E+04	561.02	7.30	-0.93	PB
L-D1	3.98E+03	1.91E+04	8.10E+04	506.45	8.15	-10.57	PB
I-D1	3.71E+03	1.76E+04	8.09E+04	261.98	3.25	-53.74	ST
H-D2	4.61E+03	2.04E+04	9.83E+04	551.95	5.50	-2.54	PI
T-D2	4.16E+03	1.98E+04	8.21E+04	572.27	8.10	1.05	PB
L-D2	4.01E+03	1.92E+04	7.83E+04	540.36	7.11	-4.58	PB
I-D2	4.36E+03	2.07E+04	8.21E+04	519.39	6.11	-8.29	PB

Table 12 Comparison between FE results and Eurocode 9, Group D

Panel ID	FEA (Ultimate load)	Eurocode 9 (Design resistance)	Bias	Safety factor

	P_u, kN	P_{EC9}, kN	(P_{EC9}/P_u)	S_f
Ref.	566.31	346.22	0.61	1.64
H-D1	525.16	340.61	0.65	1.54
T-D1	561.02	267.09	0.48	2.10
L-D1	506.45	238.82	0.47	2.12
I-D1	261.98	108.42	0.41	2.42
H-D2	551.95	398.13	0.72	1.39
T-D2	572.27	307.23	0.54	1.86
L-D2	540.36	278.63	0.52	1.94
I-D2	519.39	261.41	0.50	1.99

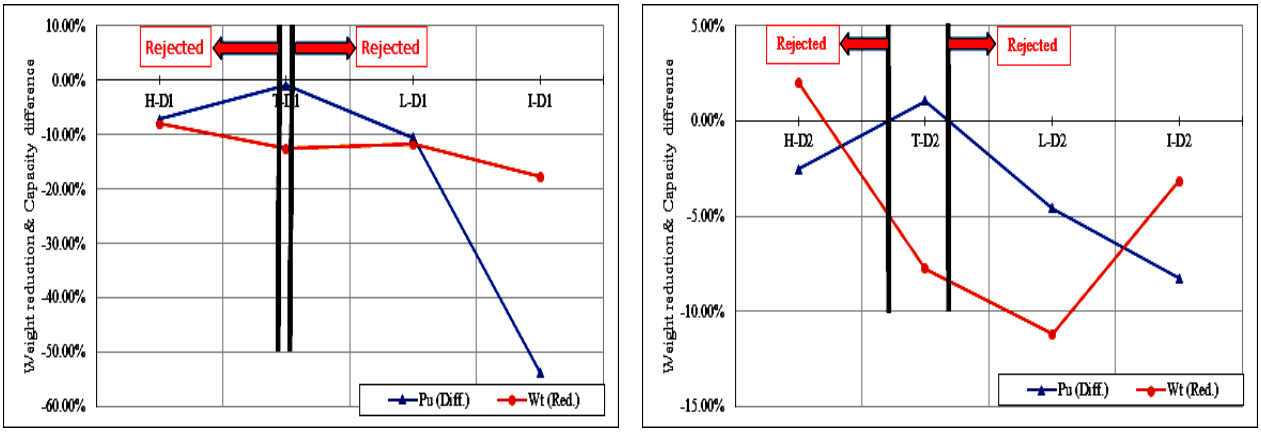

Fig. 20 Proposed criteria to select the optimum extruded section, Group D1 (left) and Group D2 (right)

3.4. FE Results for Group E

In the last group of the analysis, the plating thickness is constant of 3 mm but both web and flange thickness are varied conditionally that; Group E1 ($t_p > t_w > t_f$), Group E2 ($t_p > t_f > t_w$), Group E3 ($t_p < t_w < t_f$) Group E4 ($t_p < t_f < t_w$). The achieved load-displacement relationship for each group is shown in Fig. 21.

It is clear that as the plating thickness is bigger than both web and flange, only T-cross sections T-E1 and T-E2 showed ultimate capacity closer to the Ref. one by -0.76% and -1.11%, respectively. On contrary, when the plating thickness is less than both web and flange, the T-cross sections T-E3 and T-E4 registered higher reduction of the ultimate capacity -4.16% 3.24 %, respectively, while the behavior of the other section improved than before, resulting in ultimate capacity of -1.81% for H-E3, with respect to the Ref. one, as presented in Fig. 22. Therefore, it may be concluded that the plating thickness plays the main role in the ultimate strength for such sections.

Based on the best section criterion, see Fig. 23, it is clear that only T-E1 and T-E2 are the best cross-sections, with better recommendation for T-E1 with -0.76% and 13.22% ultimate capacity and weight reduction with respect to the Ref. one. It may be noticed that H-E4 registered ultimate capacity of -1.81% regarding the Ref., which is within the accepted range, but on contrary, this section shows higher weight than the ref. one by 4.60%, therefore, this section is rejected, see Fig. 23.

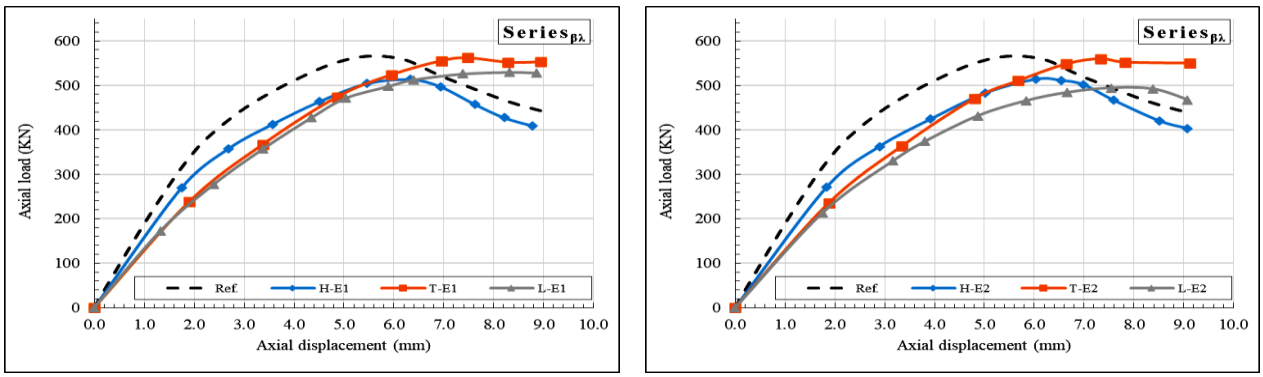

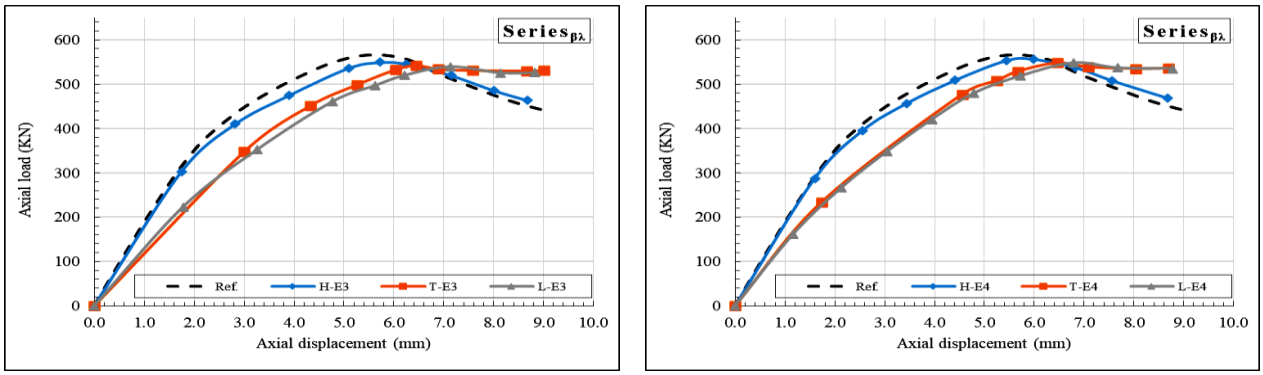

Fig. 21 Load shortening curve for Group E

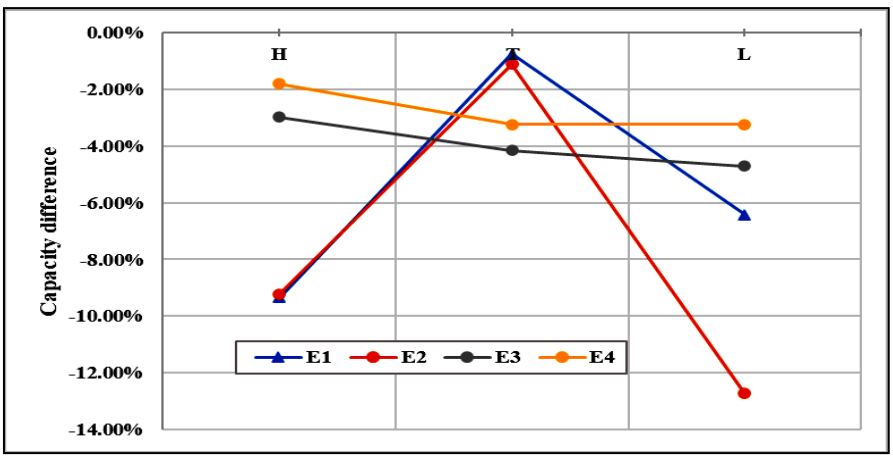

Fig. 22 Plot of the capacity difference for each cross-section, Group E

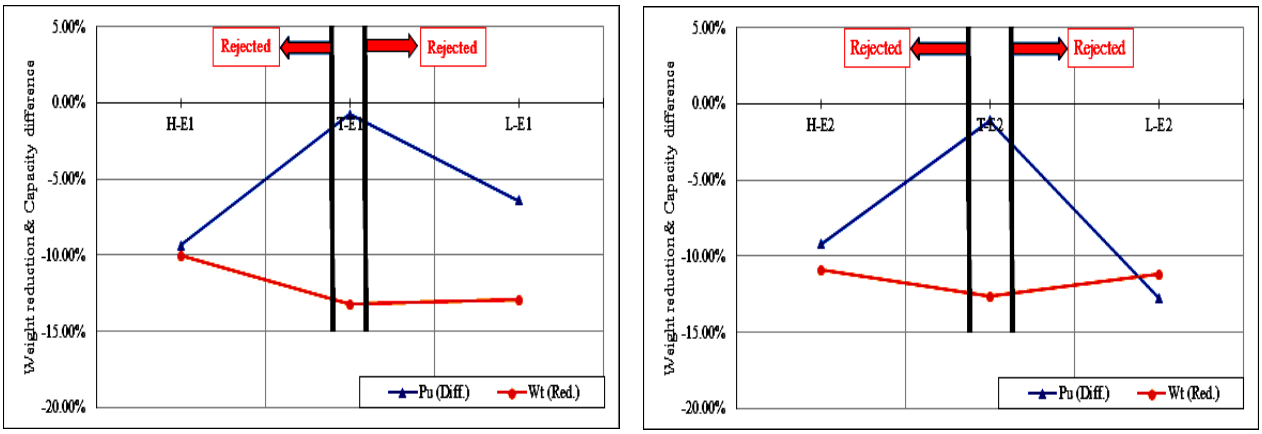

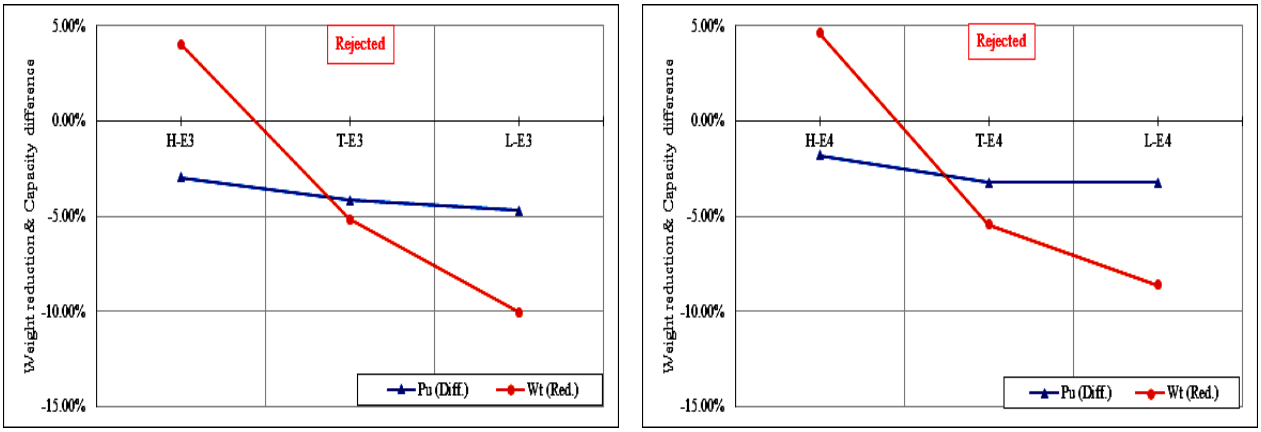

Fig. 23 Proposed criteria to select the optimum extruded section, Group E

4. CONCLUSION

A series of finite element analysis has been conducted for aluminum stiffened panel to find out the best aluminum extruded profiles (HAT, TEE, ANGLE and FLAT bar) in alloy 6082-T6 based on different panel geometrical properties. Based on the performed analysis a criterion has be proposed for selecting the best cross-section considering both load carrying capacity and cross-section weight. Also, a comparison between the resultant ultimate capacity and Eurocode 9 has been performed. It has been concluded that the optimal section for the current analysis is a T-section with plate, web, and flange of the same thickness; this section shows a higher ultimate capacity of 1.27% and weight reduction of 12.07%, while the flat bar is not a comparable extruded profile. It has to be stressed that the proposed criterion benefits both design and production strategies for marine aluminum stiffened panels.

CREDIT AUTHORSHIP CONTRIBUTION STATEMENT:
M. A. El-malaki: Modelling, Analysis and Editing, **S. Saad-Eldeen:** Concept, Methodology and Reviewing, **H.S. El-Kilani:** Concept, Methodology and Reviewing.

DECLARATION OF COMPETING INTEREST: The authors declare that they have no known competing financial interests or personal relationships that could have appeared to influence the work reported in this paper.

5. REFERENCES

[1] G. Little, "Collapse behaviour of aluminium plates," International Journal of Mechanical Sciences, vol. 24, no. 1, pp. 37-45, 1982.

[2] R. Butler, M. Lillico, G. Hunt, and N. McDonald, "Experiments on interactive buckling in optimized stiffened panels," Structural Multidisciplinary Optimization, vol. 23, no. 1, pp. 40-48, 2001.

[3] J. K. Paik, C. Andrieu, and H. Paul Cojeen, "Mechanical Collapse Testing on Aluminum Stiffened Plate Structures for Marine Applications," in 10th International Symposium on Practical Design of Ships and Other Floating Structures, Houston, Texas, United States of America, 2007: American Bureau of Shipping.

[4] M. R. Khedmati, M. R. Zareei, and P. Rigo, "Sensitivity analysis on the elastic buckling and ultimate strength of continuous stiffened aluminium plates under combined in-plane compression and lateral pressure," Thin-Walled Structures, vol. 47, no. 11, pp. 1232-1245, 2009.

[5] L. Rønning, A. Aalberg, and P. K. Larsen, "An experimental study of ultimate compressive strength of transversely stiffened aluminium panels," Thin-Walled Structures, vol. 48, no. 6, pp. 357-372, 2010.

[6] M. R. Zareei, M. R. Khedmati, and P. Rigo, "Application of artificial neural networks to the evaluation of the ultimate strength of uniaxially compressed welded stiffened aluminium plates," Proceedings of the Institution of Mechanical Engineers, vol. 226, no. 3, pp. 197-213, 2012.

[7] S. Tawosy, R. Ramadan, M. Mansour, and H. S. El-Kilani, "Ultimate Strength behavior of Aluminum Stiffened Panel under Combined Load," Port-Said Engineering Research Journal, vol. 22, no. 2, pp. 46-55, 2018.

[8] M. Mohammadi, M. R. Khedmati, and E. Bahmyari, "Elastic local buckling strength analysis of stiffened aluminium plates with an

emphasis on the initial deflections and welding residual stresses," Ships and offshore structures, vol. 14, no. 2, pp. 125-140, 2019.
[9] T. Tryland, O. S. Hopperstad, and M. Langseth, "Design of experiments to identify material properties," Materials Design, vol. 21, no. 5, pp. 477-492, 2000.
[10] Eurocode 9: Design of Aluminium structures, 2011.
[11] L. Gardner and M. Theofanous, "Discrete and continuous treatment of local buckling in stainless steel elements," Journal of Constructional Steel Research, vol. 64, no. 11, pp. 1207-1216, 2008.
[12] M.-N. Su, B. Young, and L. Gardner, "Classification of aluminium alloy cross-sections," Engineering Structures, vol. 141, pp. 29-40, 2017.
[13] B. Liu, Y. Garbatov, W. Wu, and C. G. Soares, "Study on Ultimate Compressive Strength of Aluminium-Alloy Plates and Stiffened Panels," Journal of Marine Science and Application, pp. 1-19, 2020.
[14] A. Aalberg, M. Langseth, and P. K. Larsen, "Stiffened aluminium panels subjected to axial compression," Thin-Walled Structures vol. 39, pp. 861–885, 2001.
[15] M. Kmiecik, "Behaviour of axially loaded simply supported long rectangular plates having initial deformations," Ship Research Institute, vol. Technical Report No. R84,Trondheim, 1971.
[16] ANSYS®, in Release 11.0 Documentation for ANSYS, ed: United States of America: ANSYS Inc., 2007.
[17] M. Collette, X. Wang, J. Li, J. Walters, and T. Yen, "Ultimate Strength and Optimization of Aluminum Extrusions," vol. SSC-454, ed: Ship Structure Committee, 2008.
[18] S. Zhu, J. Yan, Z. Chen, M. Tong, and Y. Wang, "Effect of the stiffener stiffness on the buckling and post-buckling behavior of stiffened composite panels – Experimental investigation," Composite Structures, vol. 120, pp. 334-345, 2015/02/01/ 2015.
[19] O. Bedair, "Analysis and limit state design of stiffened plates and shells: A world view," Applied Mechanics Reviews, vol. 62, no. 2, 2009.
[20] SSC, "Ultimate Strength and Optimization of Aluminum Extrusions," 2008.
[21] P. Rigo et al., "Sensitivity analysis on ultimate strength of aluminium stiffened panels," Marine Structures, vol. 16, no. 6, pp. 437-468, 2003.